American Mineralogist, Volume 95, pages 1017–1026, 2010

Determination of nanoparticulate magnetite stoichiometry by Mössbauer spectroscopy, acidic dissolution, and powder X-ray diffraction: A critical review

CHRISTOPHER A. GORSKI AND MICHELLE M. SCHERER*

Civil and Environmental Engineering, University of Iowa, Iowa City, Iowa 52240, U.S.A.

ABSTRACT

A solid solution can exist of magnetite (Fe_3O_4) and maghemite (γ-Fe_2O_3), which is commonly referred to as nonstoichiometric or partially oxidized magnetite. The degree of stoichiometry in magnetite is quantitatively measured by determining the ratio of Fe^{2+} to Fe^{3+}. Magnetite stoichiometry (x = Fe^{2+}/Fe^{3+}) strongly influences several physical properties, including the coercitivity, sorption capacity, reduction potential, and crystalline structure. Magnetite stoichiometry has been extensively studied, although very little work exists examining the stoichiometry of nanoparticulate samples (<<100 nm); when the stoichiometry was measured for nanoparticulate samples, it was not validated with a secondary technique. Here, we review the three most common techniques to determine magnetite stoichiometry: (1) acidic dissolution; (2) Mössbauer spectroscopy; and (3) powder X-ray diffraction (pXRD), specifically with nanoparticulate samples in mind. Eight samples of nonstoichiometric magnetite were synthesized with x ranging from 0 to 0.50 and with the particle size kept as similar as possible (BET specific surface area = 63 ± 7 m^2/g; particle size ≈ 20 nm). Our measurements indicate excellent agreement between stoichiometries determined from Mössbauer spectra and by acidic dissolution, suggesting that Mössbauer spectroscopy may be a useful means for estimating magnetite stoichiometry in nanoparticulate, multi-phases samples, such as those found in the environment. A significant linear correlation was also observed between the unit-cell length (a) of magnetite measured by pXRD and magnetite stoichiometry, indicating that pXRD may also be useful for determining particle stoichiometry, especially for mixed phased samples.

Keywords: Magnetite, maghemite, magnetite oxidation, nonstoichiometric magnetite, nanoparticle, Mössbauer spectroscopy, stoichiometry, X-ray diffraction

INTRODUCTION

Magnetite (Fe_3O_4) is an important mineral to several fields of study. It has widespread uses in industrial processes as a ferrofluid, including digital media recording and drug delivery (Pankhurst et al. 2003; Raj and Moskowitz 1990). Magnetite is of great interest to physicists, as it has unique magnetic properties, undergoes the Verwey transition, and is a conductor (Garcia and Subias 2004; Goss 1988; Sherman 1987; Walz 2002). Magnetite is also widely used in water treatment as an effective sorbent for many contaminants that can be easily separated from water using an applied magnet field (Yavuz et al. 2006). In corrosive environments, magnetite is a frequently observed product of steel oxidation (Stratmann et al. 1983). In natural environments, magnetite is a common end product of biological and abiotic reduction of ferric (Fe^{3+}) oxides (Hansel et al. 2005; McCormick et al. 2002; Tamaura et al. 1983), and a facile reductant for several environmental contaminants found in groundwater (Gorski and Scherer 2009; Lee and Batchelor 2002; McCormick et al. 2002; Scott et al. 2005; White and Peterson 1996).

Magnetite has an inverse spinel structure (space group *Fd*3*m*), which has an oxygen cubic closed-packed structure, and a 2:1 octahedral (Oct) to tetrahedral (Tet) site occupancy with Fe atoms. As a result, the magnetite formula can be written more precisely as $^{Tet}Fe^{3+}[^{Oct}Fe^{2+}Fe^{3+}]O_4$. In the literature, the ^{Tet}Fe is often referred to as the "A" site, and the ^{Oct}Fe is denoted as the "B" site. For clarity of discussion, we will refer to these sites as Oct and Tet throughout this paper. Within the unit cell, there are eight $^{Tet}Fe^{3+}$, eight $^{Oct}Fe^{2+}$, eight $^{Oct}Fe^{3+}$, and 32 O atoms.

Magnetite can have a range of oxidation states dependent upon the amount of structural Fe^{2+}, which can be discussed quantitatively as the magnetite stoichiometry (x = Fe^{2+}/Fe^{3+}). For magnetite with an ideal Fe^{2+} content (assuming the Fe_3O_4 formula), the mineral phase is known as stoichiometric magnetite (x = 0.50). As magnetite becomes oxidized, the Fe^{2+}/Fe^{3+} ratio decreases (x < 0.50), with this form denoted as nonstoichiometric or partially oxidized magnetite. When the magnetite is completely oxidized (x = 0), the mineral is known as maghemite (γ-Fe_2O_3). For nonstoichiometric magnetite, the structure is often written as $Fe_{3-\delta}O_4$, where δ can range from zero (stoichiometric magnetite) to $^1/_3$ (completely oxidized). This formula can be expressed as $^{Tet}Fe^{3+}[^{Oct}Fe^{2+}_{1-3\delta}Fe^{3+}_{1+2\delta}\square_\delta]O_4$, where $\square$ are vacancies formed in the crystal structure to account for charge balance. Note that this model assumes that all vacancies occur in Oct sites, which is a topic of debate in the literature (da Costa et al. 1996; Goss 1988; Tronc et al. 1982). The stoichiometry can easily be converted to and from this form by the following relationship:

$$x = \frac{Fe^{2+}}{Fe^{3+}} = \frac{1-3\delta}{2+2\delta} \quad . \tag{1}$$

The magnetite stoichiometry can dramatically influence the particles' physical and chemical properties, including the reduc-

* E-mail: michelle-scherer@uiowa.edu

tion potential (Gorski et al. 2010; Stockbridge et al. 1961; White et al. 1994), conductivity (Itai et al. 1971; Verwey and Haayman 1941), and crystalline structure (e.g., Annersten and Hafner 1973). In our previous work, we demonstrated that stoichiometry influences the measured open-circuit potential (E_{OCP}), as well as the reactivity of magnetite with nitrobenzene and dissolved Fe^{2+} (Gorski et al. 2010; Gorski and Scherer 2009). Magnetite stoichiometry is important to several other fields as well, as it influences the sorption capacity for heavy metals (Peterson et al. 1997), and affects the coercitivty, a property critical to digital data storage (Goss 1988).

Due to the large influence of stoichiometry on the physical properties of magnetite, it is critical to measure the stoichiometry both accurately and precisely. The most common methods for measuring magnetite stoichiometry include: (1) ^{57}Fe Mössbauer spectroscopy (da Costa et al. 1995; Daniels and Rosencwaig 1969; Schmidbauer and Keller 2006; Vandenberghe and de Grave 1989; Volenik et al. 1975); (2) complete acidic dissolution (Annersten and Hafner 1973; Gorski and Scherer 2009; Jolivet et al. 1992; Tronc et al. 1989; Volenik et al. 1975); and (3) powder X-ray diffraction (pXRD) (da Costa et al. 1995; Gallagher et al. 1968; Jolivet and Tronc 1988; Schmidbauer and Keller 2006; Tronc et al. 1992; Volenik et al. 1975; Yang et al. 2004). Other less common spectroscopic techniques have also been used to characterized stoichiometry, including X-ray magnetic circular dichroism (XMCD) and Fourier transform infrared spectroscopy (FTIR) (Antonov et al. 2003; Carvallo et al. 2008; Gotic et al. 2009; Morrall et al. 2003).

Studies measuring magnetite stoichiometry are often done on large particulate magnetite, with particle sizes typically being larger than those of nanoparticulates (≥100 nm) (da Costa et al. 1995; Daniels and Rosencwaig 1969; Gotic et al. 2009; Ramdani et al. 1987; Schmidbauer and Keller 2006; Volenik et al. 1975; Yang et al. 2004). In corrosion, environmental, and geochemical studies, however, nanoparticulate magnetite (<<100 nm) is often examined due to it being more representative of samples collected in the environment (Cornell and Schwertmann 2003; Ferrey et al. 2004; Vikesland et al. 2007). As a result, it is difficult to access if the classic techniques for measuring stoichiometry of large particulate samples can be accurately applied to nanoparticulate samples. For example, room-temperature Mössbauer spectra of magnetite are often used to extract the stoichiometry of magnetite, yet similar room-temperature spectra of nanoparticulate samples cannot be fit due to the size-dependent magnetic behavior that arises within the sample (i.e., superparamagnetism) (e.g., da Costa et al. 1996). Similarly, it is unclear if the unit-cell parameters and peak intensities extracted from fitted pXRD patterns are influenced by nanoparticulate effects (Reynolds 1989). In the few cases where the stoichiometry was determined for nanoparticulate samples (Jolivet et al. 1992; Tronc et al. 1989), the stoichiometry was not measured with a secondary technique, making it difficult to access the accuracy, precision, and possible bias of these singular measurements.

Here, we measured the stoichiometry of eight nanoparticulate magnetite (~20 nm particles) samples using three measurement techniques: acidic dissolution (x_d), Mössbauer spectroscopy (x_{MS}), and pXRD. Magnetite stoichiometries determine by Mössbauer spectroscopy (x_{MS}) are typically determined from room-temperature (298 K) spectra, but nanoparticulate magnetite does not produce well-resolved spectra at this temperature. We overcame this issue by selecting a colder temperature of 140 K to collect and fit spectra for nanoparticulate magnetite and using recently developed modeling techniques. We found excellent agreement between x_d and x_{MS}, with no observable bias in either method. We also used pXRD to characterize the samples to determine relative peak intensity and the fitted unit-cell length (a) as a function of x_d. We examined the general trends between stoichiometry and pXRD fitted results with our samples as well as literature values for magnetite samples with a wide range of particle sizes. Our observations indicated that the particle size does not influence the observed trend between the unit-cell length (a) and the stoichiometry, although trends between peak intensity and stoichiometry were not observed here. This data suggests that pXRD may be a useful technique for determining nanoparticulate magnetite stoichiometry, although pXRD is likely to be less precise than acidic dissolution and Mössbauer spectroscopy.

Materials and experimental methods

Magnetite synthesis and characterization

Stoichiometric nanoparticulate magnetite was synthesized by creating a 2:1 Fe^{2+}:Fe^{3+} acidic solution (pH < 1) in an anaerobic N_2/H_2 (94/6) glovebox. The solution was then titrated to an alkaline pH (10–11) using 5 *M* NaOH, while being stirred and allowed to mix overnight (adapted from Schwertmann and Cornell 1991). To form nonstoichiometric magnetite, concentrated H_2O_2 was added to the solution after the overnight equilibration and allowed to equilibrate an additional day. For all batches, the resultant solution was filtered within the glovebox, with minimal washing used (1 rinse), as additional washing resulted in oxidation of stoichiometric magnetite due to Fe^{2+} dissolution. The solids were then freeze-dried outside the glovebox, and were then returned to the glovebox for sieving (100 mesh) and storage prior to characterization. Maghemite was synthesized from magnetite by baking it at 200 °C for 2 h outside the glovebox (Schwertmann and Cornell 1991).

Particles were characterized by acidic dissolution (x_d), ^{57}Fe Mössbauer spectroscopy (x_{MS}), pXRD, BET, and some samples were examined using surface and transmission electron diffraction (SEM and TEM). BET specific surfaces areas (SSA) were 63 ± 7 m^2/g, and have been provided for each batch in our previous works (Gorski et al. 2010; Gorski and Scherer 2009). TEM images showed spherical particles that were approximately 20 nm in diameter, in good agreement with the size expected from the BET SSA (Gorski et al. 2010; Gorski and Scherer 2009). There were no discernable trends between the stoichiometry and the particle morphology or size.

The large particulate magnetite was prepared from a natural magnetite single crystal from Minas Gerais, Brazil (Ward's Natural Science, Rochester, New York, U.S.A.). The sample was ground in a mortar and passed through a 100 mesh sieve in an anaerobic glovebox. The sample was characterized by dissolution, Mössbauer spectroscopy, and pXRD. The particle size was determined to be large (>200 nm) based on the pXRD patterns using the Scherrer equation.

Acid dissolution method

The dissolution stoichiometries ($x_d = Fe^{2+}/Fe^{3+}$) were determined by dissolving the solids in 5 *M* HCl in an anaerobic N_2/H_2 glovebox. The target total Fe concentration was 10 *mM*. The nanoparticulate solids took approximately 2–4 h to completely dissolve, while the large particulate sample took several days. The Fe^{2+} and total Fe concentrations were then measured using the phenanthroline method (Tamura et al. 1974). The standard deviation was low between replicate samples (σ_d < 0.01). Note that filtering the acidic Fe solutions at any stage of analysis significantly oxidized the dissolved Fe^{2+}, which was likely due to nitrate groups present on the filter paper.

Mössbauer spectroscopy

Transmission Mössbauer spectroscopy was performed with a variable temperature He-cooled system with a 1024 channel detector. The ^{57}Co source used (~50 mCi) was in an Rh matrix at room temperature. All center shifts reported are relative to α-Fe foil at room temperature. Samples were prepared by sealing the powder specimen between two pieces of 5 mL Kapton tape to avoid oxidation

while mounting the sample.

Spectral fitting was done using Recoil Software (University of Ottawa, Ottawa, Canada). Lorentzian, Voigt, and extended-Voigt fits were used to model the spectra to determine the most accurate model. Unless noted, all fits presented were done with extended-Voigt fitting. For all fits, the relative sextet peak areas (3:2:1:1:2:3) were held constant. The Lorentzian linewidth was held at 0.12 mm/s for Voigt and extended-Voigt fitting, as it was the linewidth measured on the spectrometer for an ideally thick α-Fe foil. For all fits, unless otherwise noted, the center shift (CS), quadrupole shift (QS), hyperfine parameter (H), and relative areas between sites were allowed to float during fitting. Both sextets had two hyperfine components that were allowed to float, as the fits were unacceptably poor when only one component was used. The CS and QS were fit with single components in all cases.

Powder X-ray diffraction

pXRD patterns were collected using a Rigaku MiniFlex II system equipped with a Co source (Co$K\alpha$ = 1.78899 Å). Sample powders were mixed with a small amount of glycerol to form a thick paste in an anaerobic glovebox to avoid inadvertent oxidation during analysis (Hansen 1989). Samples were analyzed from 5–80 °2θ with a 0.02° step size and a 1.2 s dwell time. Patterns were analyzed and fit using Jade 6 software (Materials Data, Incorporated, U.S.A.). For analysis, patterns were smoothed, background subtracted, and $K\alpha_2$ stripped prior to analysis and fitting. A broad peak was observed at approximately 24 °2θ due to the glycerol, otherwise all the peaks were characteristic of magnetite. Fitting was done using pseudo-Voigt peaks with allowable displacement error to minimize error as outlined elsewhere (Howard and Preston 1989).

Results and discussion

Mössbauer characterization of stoichiometric magnetite

Mössbauer spectra collected for a large particulate (>200 nm) and a nanoparticulate (~20 nm) stoichiometric magnetite (x_d = 0.50) at a series of temperatures ranging from room temperature (298 K) to 13 K are shown in Figure 1. Mössbauer temperature profiles are a useful method for characterizing iron minerals because their magnetic behaviors, and subsequently observed spectra, are highly temperature dependent as can be seen by the change in peak localities and intensities in Figure 1.

For large particulate and single-crystal samples of magnetite, two primary temperature domains exist at and below room temperature. From room temperature down to 121 K, a Mössbauer spectrum of magnetite is characterized by two sextets. For the large particulate magnetite spectrum at 298 K in Figure 1, the left-hand side of the spectrum shows two clearly defined sextets, which overlap on the right-hand side of the spectrum. For stoichiometric (x = 0.50), these two sextets correspond to the $^{Tet}Fe^{3+}$ and the $^{Oct}Fe^{3+}$ and $^{Oct}Fe^{2+}$. Magnetite, which is a conductor, exhibits rapid electron hopping between the $^{Oct}Fe^{3+}$ and $^{Oct}Fe^{2+}$ at room temperature, which is faster than the characteristic sample time for Mössbauer spectroscopy (10^{-8} s). As a result of this fast electron hopping, the ^{Oct}Fe atoms are observed with an average valence state of 2.5+, with the sextet referred to as $^{Oct}Fe^{2.5+}$. For samples that are partially oxidized (x < 0.50), an $^{Oct}Fe^{3+}$ sextet is present in the spectrum, which closely overlaps with the $^{Tet}Fe^{3+}$ sextet. When an external magnetic field is used with Mössbauer spectroscopy, the two signals ($^{Oct}Fe^{3+}$ and $^{Tet}Fe^{3+}$) can be discerned; however, in the absence of an external magnetic field, they are typically modeled as one site (Daniels and Rosencwaig 1969; Vandenberghe et al. 2000; Vandenberghe and de Grave 1989). In the absence of an external magnet, 298 K magnetite spectra are often fit to extract the stoichiometry by comparing the relative areas of the $^{Oct,Tet}Fe^{3+}$ and the $^{Oct}Fe^{2.5+}$ using the following equation (da Costa et al. 1995; Daniels and Rosencwaig 1969; Vandenberghe and de Grave 1989):

$$x_{MS} = \frac{Fe^{2+}}{Fe^{3+}} = \frac{\frac{1}{2}{}^{Oct}Fe^{2.5+}}{\frac{1}{2}{}^{Oct}Fe^{2.5+} + {}^{Oct,Tet}Fe^{3+}}. \quad (2)$$

In Figure 1, the room-temperature spectrum of the nanoparticulate magnetite (right) is significantly different than the large particulate magnetite (left). For the nanoparticulate sample, two sextets are still visibly present, but the sextets are significantly broader and overlap considerably. The change in the Mössbauer spectrum is due to the small particle size, which can cause a greater distribution in magnetic behavior due to a higher percentage of surface atoms, additional stresses between atoms, and superparamagnetic behavior due to the small domain sizes (da Costa et al. 1995; Degrave et al. 1993; Lotgering and Vandiepen 1977; Morrish et al. 1976). Similar room-temperature spectra have been previously observed for nanoparticulate magnetite (Jolivet et al. 1992; Jolivet and Tronc 1988; Tronc et al. 1989). The overlapping sextets make it difficult to fit the spectrum, and our attempts to do so resulted in non-unique fits (i.e., different x_{MS} values) depending on the initial assumptions used. Note that some previous work has used 298 K fits of nanoparticulate magnetite to determine stoichiometry, despite the difficulty and ambiguity of fitting (Jolivet and Tronc 1988).

Upon cooling the magnetite sample, both the large particulate and nanoparticulate magnetite spectral features change considerably (Fig. 1). At 200 and 140 K, the large particulate magnetite spectra look similar to the room-temperature spectrum, however the inner sextet ($^{Oct}Fe^{2.5+}$) broadens. For the nanoparticulate sample, the spectra become better resolved upon cooling, as the size-dependent effects become less pronounced. The 200

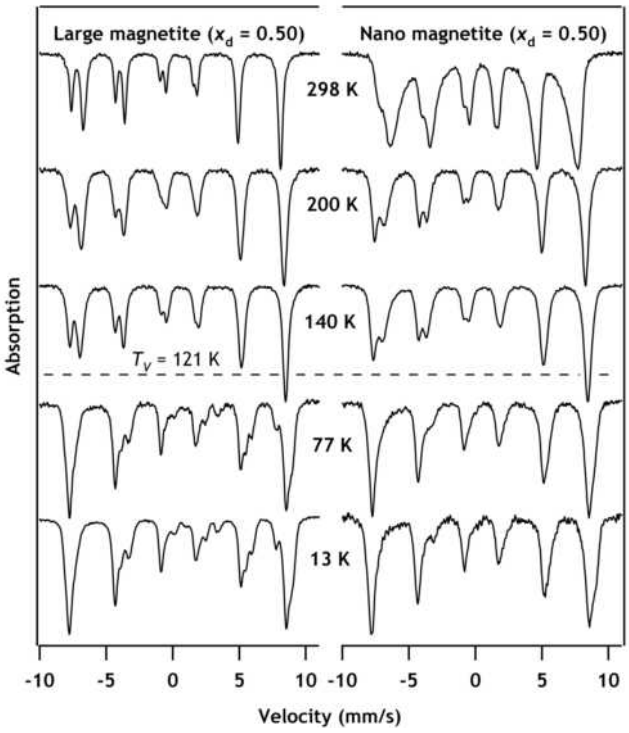

Figure 1. Mössbauer spectra of large particulate and nanoparticulate stoichiometric magnetite (x_d = 0.50) at several temperatures (298, 200, 140, 77, and 13 K).

and 140 K spectra look similar to those of the large particulate magnetite; however, the $^{Oct}Fe^{2.5+}$ sextet is broader for the nanoparticulate sample.

Upon cooling the magnetite sample further, a distinct change in the magnetic properties occurs at 121 K, which is known as the Verwey transition point (T_V). Below this temperature, the conductivity of magnetite is significantly reduced, and the magnetic behavior dramatically changes (Garcia and Subias 2004; Walz 2002). The cause for these changes is a controversial subject in the literature, and, despite extensive work, a consensus has yet to be reached. The effect of transition can be seen clearly for the large particulate magnetite in Figure 1, where several additional peaks can be seen in the 77 and 13 K spectra. For the nanoparticulate magnetite, the 77 and 13 K spectra also look considerably different with peaks absent that are present for the large particulate magnetite. From these spectra, is unclear if the nanoparticulate magnetite does not undergo the Verwey transition, or, if the Verwey transition does occur, the resultant spectra are different due to the small particle size. In one study, it was shown that the Verwey transition is highly dependent upon stoichiometry, but not of particle size (Ozdemir et al. 1993); however, in that study, their small particulate magnetite (0.22 μm) was not a nanoparticulate sample (<100 nm), and was similar in size to our large particulate sample.

Determining magnetite stoichiometry from Mössbauer spectra

Based on the temperature-dependent behavior shown in Figure 1, we chose to use spectra collected at 140 K to determine the stoichiometry of nanoparticulate magnetite. Our goal was to evaluate whether Mössbauer spectroscopy could be used to reliably estimate the stoichiometry of nanoparticulate magnetite by comparing the stoichiometry measured by acidic dissolution (x_d) and Mössbauer spectroscopy (x_{MS}). Note that for large particulate magnetite, a room-temperature spectrum is often used and is sufficient to calculate the stoichiometry using the relative areas of the two sextets. For nanoparticulate magnetite, however, the room-temperature spectrum is complicated and fitting does not provide a unique set of parameters. Spectra collected at 140 K were the best candidates because the temperature was low enough to minimize the nanoparticulate superparamagnetic effects and high enough (>121 K) to avoid complications arising from the Verwey transition. Figure 2 contains model fits for 140 K spectra for the large particulate and nanoparticulate magnetite. Despite the effects of cooling to reduce the influence of particle size, there are still discernable differences, such as the $^{Oct}Fe^{2.5+}$ sextet is much broader for the nanoparticulate sample.

In addition to the relative abundance of phases within a sample, spectral fitting provides additional parameters: the center shift (CS), the quadrupole shift (QS), and the hyperfine field (H), which are collectively known as the hyperfine parameters, and measure the nucleus-electron interactions. Each hyperfine parameter related closely to physical properties of the sample. The center shift is proportional to the electron density for the Fe atom, with an Fe^{2+} atom having a lower electron density than an Fe^{3+} atom due to extra d-electron reducing s-electron density, and thus the center shift of an Fe^{2+} atom is higher than an Fe^{3+} atom in most cases. For the $^{Oct}Fe^{2.5+}$ sextet, the observed center shift is a combination of the Fe^{2+} and Fe^{3+}, and is higher (~0.72 mm/s at 140 K) than the $^{Tet}Fe^{3+}$ sextet (~0.37 mm/s at 140 K). The quadrupole shift is proportional to the relative bond symmetry of an Fe atom, with higher stresses and strains resulting in a larger quadrupole shift. For a perfectly symmetrical atom, like the $^{Tet}Fe^{3+}$ in magnetite, the expected quadrupole shift should be zero. The hyperfine field is proportional to the strength of the internal magnetic field (in the absence of an applied field). For nanoparticles, the hyperfine field is typically smaller than their large particulate analogs due to poorer ordering of spins within the lattice (da Costa et al. 1996). Here, we observe significantly smaller hyperfine field values for the nanoparticulate phases.

Two fundamentally different models exist for extracting the hyperfine parameters from a Mössbauer spectrum: Lorentzian and Voigt-based. For a Lorentzian fit, the width of the peaks is accounted for by broadening a single Lorentizan peak; in the Voigt model, however, the peak is modeled as a Gaussian distribution of several Lorentzian peaks resulting from multiple unique atomic sites within the sample. This difference is not subtle, as it changes the shape of the peaks, and results in different fits and extractable parameters. Rancourt and co-workers have argued extensively for the merit of the Voigt-based model, citing that floating the Lorentzian linewidth is a physically incorrect assumption (Lagarec and Rancourt 1997; Ping and Rancourt 1994a, 1994b; Rancourt and Ping 1991). Previous work has often assumed a Lorentzian model to fit the peak profiles (Daniels and Rosencwaig 1969; Haggstrom et al. 1978; Vandenberghe and de Grave 1989), which has worked well for large particulate magnetite due to the samples being well-crystalline, which results in a narrow distribution of sites (and negligible Voigt distribution). The Lorentzian fitting model could not be applied to the nanoparticulate magnetite in this study, however, because the peak shapes were distinctly non-Lorentzian in shape. A Voigt model was required to achieve reasonable fits that captured the peak shape and distributions of the spectra. For example, Lorentzian modeling of the spectra in Figure 2 resulted in x_{MS} values for

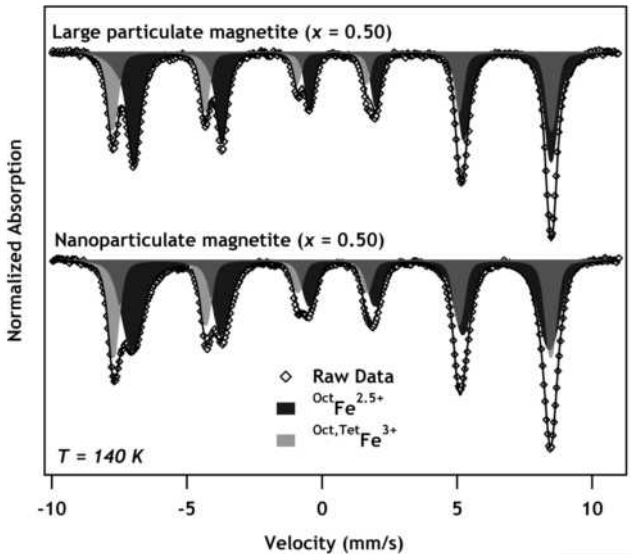

FIGURE 2. Fitted Mössbauer spectra of stoichiometric large particulate magnetite (top) and nanoparticulate magnetite (bottom) collected at 140 K. Fit parameters are shown in Table 1.

both the large particulate and nanoparticulate magnetite that were lower than the x_d value of 0.50. The discrepancy was much greater for the nanoparticulate magnetite, with an x_{MS} of only 0.27, and an x_{MS} of 0.44 for the large particulate sample. Modeling the spectra with the Voigt model provided x_{MS} values of 0.50 (large particulate) and 0.47 (nanoparticulate), which were much closer to the x_d of 0.50 (Fig. 2). Our results suggest that for nanoparticulate magnetite, it is important to use appropriate fitting models, such as Voigt-based models, when estimating stoichiometry from Mössbauer spectroscopy.

Another consideration is that the spectral areas in a Mössbauer spectrum do not always directly correlate to the relative abundance of sites because some of the sites are not completely rigid (i.e., they have some recoil). The percentage of Fe atoms that are rigid enough to undergo the necessary nuclear absorption and emission process, which results in an absorption Mössbauer spectrum is known as the recoilless fraction (*f*). In a previous study, a room-temperature recoilless fraction ratio ($f_{2.5+}/f_{3+}$) of 0.94 was determined (Sawatzky et al. 1969). More recently, others have found the $f_{2.5+}/f_{3+}$ ratio is closer to 1.00 (Annersten and Hafner 1973; Volenik et al. 1975). As the temperature cools in a sample, the *f* ratio should approach 1.00 (Sawatzky et al. 1969), although this has not been experimentally validated for magnetite. The *f* ratio is critical to for extracting x_{MS}, as the spectral areas would need to be corrected for the recoilless fraction. To determine the *f* ratio for our large particulate sample, the relative areas of the two sextets ($^{Oct}Fe^{2.5+}/^{Oct,Tet}Fe^{3+}$) were fit at 298, 200, and 140 K; the relative areas were modeled to be 1.976 (298 K), 1.955 (200 K), 1.976 (140 K) (data not shown), indicating that $f_{2.5+}/f_{3+}$ is independent of temperature using this fitting method, and is likely very near to 1.00 at temperatures up to 298 K for the large particulate sample. A similar method could not be applied to the nanoparticulate samples, because fitting could only be done in a narrow temperature range, so it must be assumed that a similar *f* ratio of 1.00 exists at 140 K.

Spectral interpretation of nanoparticulate, non-stoichiometric magnetite

Spectra of nanoparticulate magnetite samples with varying stoichiometries collected at 140 K are presented in Figure 3. The Mössbauer fit parameters are shown in Table 1 with literature values at similar temperatures. As the sample becomes more oxidized (smaller *x*), the $^{Oct}Fe^{2.5+}$ sextet area decreases and the $^{Oct,Tet}Fe^{3+}$ sextet area increases. Model parameters found for the x_d = 0.50 magnetite were used as initial values for fits of the nonstoichiometric samples. For some spectra (indicated in Table 1), the center shift (CS) of the $^{Oct}Fe^{2.5+}$ sextet was fixed as 0.72 mm/s, as floating the value led to unrealistic values as discussed later.

A comparison of the stoichiometry determined by acidic dissolution (x_d) and by Mössbauer spectroscopy (x_{MS}) is shown in Figure 4. For the entire range of stoichiometry, the agreement between x_d and x_{MS} is excellent. The slope of the line is close to 1.0 indicating near-perfect agreement between x_d and x_{MS} [m = 0.96 ± 0.04 (±σ); R^2 = 0.998, n = 8]. There does not appear to be an indication of a systematic bias in either direction (i.e., overestimation or underestimation), suggesting that the fitting model used is robust, and can be applied to nanoparticulate samples over the full range of stoichiometry, that is, from maghemite to stoichiometric magnetite.

It is worth noting that in previous works, the reliability of determining the stoichiometry by acidic dissolution (x_d) has been questioned due to the possibility of inadvertent oxidation in the dissolution process (da Costa et al. 1995; Ramdani et al. 1987). As a result, the excellent agreement between x_{MS} and x_d observed here provides validation of both techniques concurrently. We suspect that since previous work was not done in an anaerobic chamber, that inadvertent oxidation reactions would be more likely. We have also found that filtering the acidic suspensions can lead to significant oxidation of Fe^{2+} if nitrate groups are present on the filter. Additionally, the use of the 1,10-phenathroline method used to measure dissolved Fe^{2+} coupled with the use of fluoride to mask the presence of Fe^{3+} greatly increased the precision of x_d (Tamura et al. 1974).

Note that we used a pair-localized model to fit the Mössbauer spectra, which explicitly assumes discernable $^{Oct}Fe^{3+}$ and $^{Oct}Fe^{2.5+}$ sites. This, however, is a controversial topic. Three models have been proposed to explain the Mössbauer spectra of non-stoichiometric magnetite above the Verwey transition: (1) the "discrete" model, where a combination of stoichiometric magnetite and maghemite is present (da Costa et al. 1995, 1996); (2) the "pair-localized" theory used here, where upon oxidation octahedral Fe^{2+} and Fe^{3+} atoms pair, with unpaired Fe^{3+} atoms resulting in the $^{Oct}Fe^{3+}$ signal (Daniels and Rosencwaig 1969; Degrave et al. 1993; Yang et al. 2004); and (3) the "band-delocalized" model, where a pool of valence electrons is shared between all ^{Oct}Fe atoms (Cullen and Callen 1970). The discrete and pair-localized

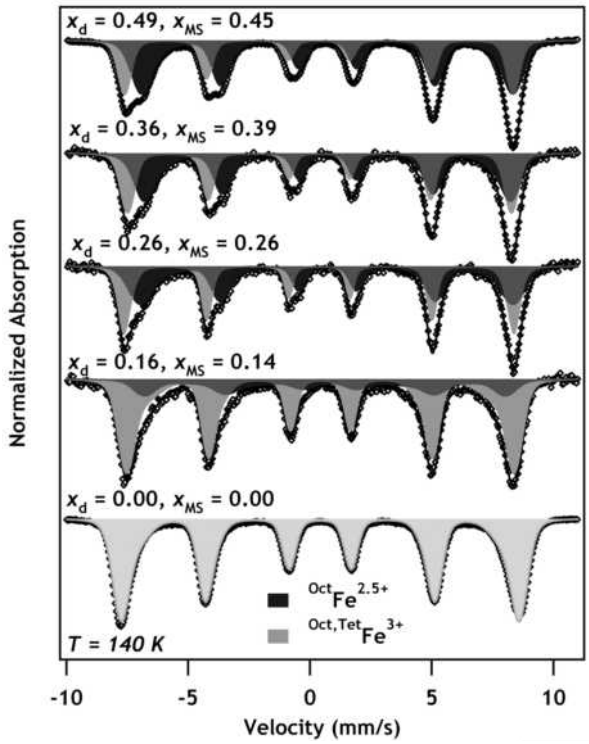

FIGURE 3. Mössbauer spectra of nanoparticulate magnetite with varying stoichiometries ($x = Fe^{2+}/Fe^{3+}$) at 140 K. The hyperfine parameters collected are shown in Table 1.

TABLE 1. Mössbauer parameters for magnetite of varying stoichiometry ($x = Fe^{2+}/Fe^{3+}$) at $T = 140$ K

		$^{Oct}Fe^{2.5+}$					$^{Tet}Fe^{3+}$,$^{Oct}Fe^{3+}$					
	x_d*	CS (mm/s)	ε (mm/s)	H (T)	st. dev. (H) (T)	Area (%)	CS (mm/s)	ε (mm/s)	H (T)	st. dev. (H) (T)	Area (%)	x_{MS}†
This work	0.00	B.D.‡	B.D.	B.D.	B.D.	0	0.42	0.00	49.8	2.5	100	0.00
	0.16	0.72§	–0.10	39.3	10.5	24.3	0.43	–0.01	48.1	3.2	75.7	0.14
	0.25	0.71	–0.03	44.0	8.4	37.7	0.40	0.00	48.8	2.3	62.3	0.23
	0.26	0.74	–0.02	46.4	4.4	41.3	0.39	–0.01	49.3	1.9	58.7	0.26
	0.36	0.72§	–0.01	45.8	3.2	56.4	0.39	0.00	48.9	1.1	43.6	0.39
	0.42	0.72	–0.02	46.8	2.5	58.5	0.37	0.00	49.5	0.8	41.5	0.41
	0.49	0.74	–0.02	46.0	3.8	62.3	0.38	0.00	49.3	0.8	37.7	0.45
	0.50	0.72	–0.02	47.4	2.8	64.1	0.38	0.00	50.2	0.1	35.9	0.47
	LP‖ (0.50)	0.76	0.00	48.2	2.1	66.4	0.37	0.00	50.4	0.6	33.6	0.50
Refs.	135 K††	0.75	–0.01	47.9	–	65	0.35	0#	50.4	–	35	0.48
	150 K‡‡	0.65	0#	46.7	–	54	0.37	0#	50.6	–	46	0.37
	130 K§§	0.68	0	47.7	–	51	0.37	0	50.8	–	49	0.34
	120 K‖‖	0.77	0	48.1##	–	38	0.34	0	50.3	–	63	0.23
	130 K***	0.76	0#	48.2	–**	64	0.35	0#	50.0	–	36	0.47

* x_d = stoichiometry determined by acidic dissolution. $\sigma_{xd} < 0.01$.
† $x_{MS} = (½\ ^{Oct}Fe^{2.5+})/(½\ ^{Oct}Fe^{2.5+} + {}^{Tet,Oct}Fe^{3+})$.
‡ B.D. = Below detection in fitting.
§ The CS was fixed at 0.72 because floating led to unrealistic parameters.
‖ LP = Large particulate magnetite.
Fixed at 0 during fitting.
** Not determined; this value is only available with Voigt-based fitting. The reference spectra were fit using Lorentzian models.
†† A synthetic well-crystalline sample (Degrave et al. 1993).
‡‡ Nanoparticulate magnetite (avg. diameter from TEM = 21 nm) produced from oxidizing nanoparticulate Fe metal via exposure to air (Kuhn et al. 2002).
§§ Natural large particulate polycrystalline magnetite taken from the Gällivare iron mine (Haggstrom et al. 1978).
‖‖ A natural soil sample containing magnetite as a constituent from Huangling, China (Vandenberghe et al. 1998).
Fit using two signals, reported value is the weighted mean of the two sextets.
*** Large particulate magnetite (particle size > 200 nm) (da Costa et al. 1995).

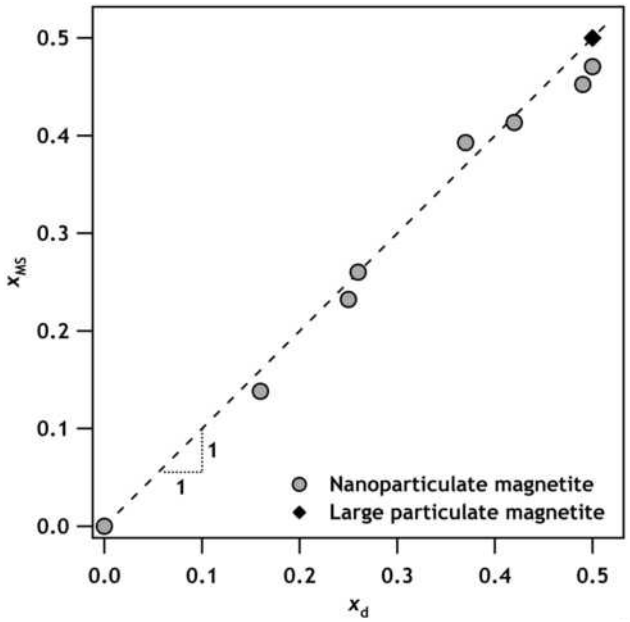

FIGURE 4. Comparison of magnetite stoichiometry determined by Mössbauer spectroscopy (x_{MS}) and acidic dissolution (x_d).

models would result in the same observed spectra with discrete $^{Oct,Tet}Fe^{3+}$ and $^{Oct}Fe^{2.5+}$ sextets, whereas the band-delocalized model would result in a $^{Tet}Fe^{3+}$ sextet and an $^{Oct}Fe^{2.z+}$ sextet, where $5 \leq z \leq 10$. It has also been hypothesized that both the pair-localized and the band-delocalized mechanisms may both be occurring simultaneously (Ihle and Lorenz 1985). In our previous work where we characterized the redox properties and reactivity of magnetite, we concluded that the discrete model [i.e., a stoichiometric magnetite core ($x = 0.5$) with a maghemite shell ($x = 0$)] is an inaccurate descriptor of nonstoichiometric nanoparticulate magnetite (Gorski et al. 2010; Gorski and Scherer 2009), and thus, we used the pair-localized model to fit the spectra here.

The good agreement between stoichiometries determined from the Mössbauer spectra and the dissolution data, however, does not necessarily imply that the pair-localized model is correct. Indeed, there are some indicators in the fit parameters (Table 1) that suggest that some band-delocalization may be occurring. For example, as the stoichiometry decreases, the $^{Oct}Fe^{2.5+}$ sextet has a lower average H, and the standard distribution [i.e., width of the sextets; std(H)] increases; this can also been seen visually in Figure 3. This suggests that the internal magnetic interactions between ^{Oct}Fe are smaller (decreasing H), and that there is a wider distribution of local ^{Oct}Fe environments [increasing std(H)]. It has also been proposed that the larger std(H) is due to slowed electron hopping rates in the conduction band, which would also manifest in widening the sextet peaks (Cullen et al. 1996; Ihle and Lorenz 1985). Others, however, have argued that these observations are also consistent with the pair-localized model, as one would expect the vacancies and reordering that must occur as Fe^{2+} atoms become Fe^{3+} will cause local disorders (Annersten and Hafner 1973; Lotgering and Vandiepen 1977).

A second indication that suggests band delocalization may be occurring is that the CS had to be fixed at 0.72 mm/s for some of the more oxidized samples (Fig. 3; Table 1) as noted earlier. Figure 5 shows the fitted spectrum for the $x_d = 0.25$ magnetite with the fixed CS (i.e., pair-localized) and without (i.e., band-delocalized). Note that the fitted areas shift substantially, and the CS drifts to 0.62 mm/s in the band-delocalized spectrum. If all the octahedral atoms were pooling electrons, an $^{Oct}Fe^{2.z+}$ sextet would be expected, and it should represent approximately two thirds of the spectral area with a minor shift due to vacancies. For the band-delocalized model, the $^{Oct}Fe^{2.z+}$ sextet accounts for only 52% of the area, so at least some of the ^{Oct}Fe is still being modeled as the $^{Oct,Tet}Fe^{3+}$ sextet. A quantitative means for com-

paring the fits is to examine the goodness-of-fit parameter, χ^2, where lower values represent a better fit. The χ^2 value is virtually identical between the samples: 1.087 for pair-localized and 1.089 for band-delocalized, indicating that one fit does not appear to model the data any better than the other. As a result, from our data, we cannot determine if the pair-localized, band-delocalized, or a combination of the two is the most accurate model to describe nonstoichiometric magnetite. We can, however, conclude that fitting the data with the pair-localized model results in excellent agreement between x_d and x_{MS}. Note that the stoichiometries cannot be determined from the fitting the data with band-delocalized model because the sextet areas would not correspond to known Fe oxidation states (i.e., 3+ and 2.z+).

Characterization of magnetite using powder X-ray diffraction

A third method that has been used to determine the stoichiometry of magnetite samples is pXRD. The pXRD pattern of magnetite has previously been shown to be dependent upon stoichiometry in several studies examining large particulate magnetite (≥100 nm) (da Costa et al. 1995; Gallagher et al. 1968; Jolivet and Tronc 1988; Tronc et al. 1992; Volenik et al. 1975; Yang et al. 2004), yet the relationship for small nanoparticulate magnetite (<<100 nm) remains largely unexplored. Stoichiometric magnetite, which has a cubic close-packed structure, has a reported unit-cell length (a) of 8.396–8.400 Å (Cornell and Schwertmann 2003; Feitknecht et al. 1962; Gotic et al. 2009; Nakagiri et al. 1986; Volenik et al. 1975). As the magnetite becomes oxidized (lower x), the unit cell becomes smaller due to the formation of vacancies and the smaller atomic size of Fe^{3+} atoms as compared to Fe^{2+}. Maghemite ($x = 0$) has a similar cubic structure, but with a slightly smaller unit-cell length (8.33–8.34 Å) (Annersten and Hafner 1973; Cornell and Schwertmann 2003; Feitknecht et al. 1962). In these studies, the stoichiometry is determined by linear interpolation between the two extreme stoichiometries (i.e., 0 and 0.5) and their reference unit-cell lengths. It has been proposed that the maghemite structure has additional symmetry due to the ordering of vacancies, which results in additional peaks observed in pXRD patterns (Gallagher et al. 1968; Tronc et al. 1982; Volenik et al. 1975). The method of maghemite preparation appears to influence the presence and intensity of these peaks, however, and it has been suggested that there are structurally different forms of maghemite with varying degrees of vacancy ordering (Annersten and Hafner 1973).

Selected pXRD patterns for magnetite over the range of stoichiometries (x_d = 0.50, 0.25, 0.00) are shown in Figure 6. The patterns have been smoothed, background-subtracted, and $K\alpha_2$-stripped to aid in interpretation. The eight most intense peaks have been labeled with their appropriate crystallographic planes (*hkl*). The patterns appear nearly identical as the changes in the unit cell are quite subtle and require fitting of peaks to extract. As the sample becomes oxidized, additional peaks are observed in both the x_d = 0.25 and 0.00 samples, which have been labeled with a star (*) for the x_d = 0.00 sample in Figure 6. Note that the small broad peak directly to the right of the (111) peak for the x_d = 0.00 is an artifact of using glycerol to avoid sample oxidation. The additional peaks observed here suggest that some vacancy ordering has occurred within the oxidized samples.

Diffraction patterns of the magnetites were fit to resolve the relative peak localities and intensities to determine if they could be used to estimate the stoichiometry of the samples. For

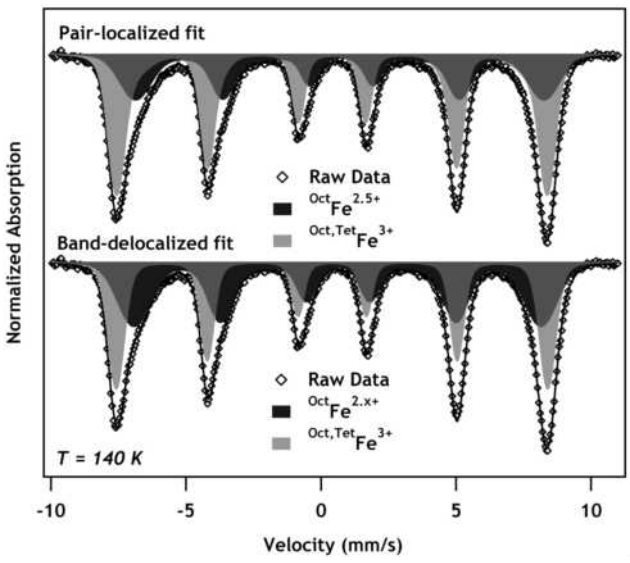

FIGURE 5. Fitted Mössbauer spectra of nonstoichiometric nanoparticulate magnetite (x_d = 0.25) collected at 140 K. The pair-localized fit assumes a CS of 0.72 mm/s (top), while the band-delocalized spectrum allows the CS to float (0.62 mm/s) (bottom).

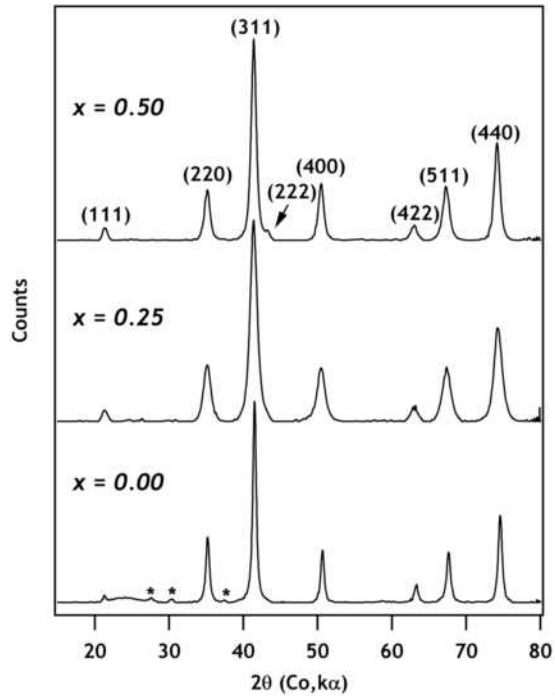

FIGURE 6. Powder X-ray diffraction of nanoparticulate stoichiometric (x = 0.50), significantly oxidized (x = 0.25), and completely oxidized (x = 0.00) magnetite. The patterns have been smoothed, background subtracted, and $K\alpha_2$ stripped to aid in interpretation. The eight most intense diffraction peaks are labeled with respect to their crystallographic planes (*hkl*). Stars (*) denote additional peaks observed in the completely oxidized sample.

the samples in Figure 6, the fitted unit-cell lengths were 8.394 Å (x_d = 0.50), 8.366 Å (0.25), and 8.339 Å (0.00). As expected, the unit-cell length decreases upon the oxidation of magnetite (which manifests in a slight left-shift of peaks in Fig. 7). The same trend has been observed by several studies in the past for large particulate (≥100 nm) samples.

The extracted unit-cell lengths are shown as a function of stoichiometry determined by acidic dissolution (x_d) in Figure 7. The peak data and resultant fits are summarized in Table 2. The error bars used for the data markers are the standard deviations provided from the fitting software with the exception of the x_d = 0.50 batch where five replicate samples were prepared, and the error bars represent the standard deviation computed from these samples. Data from previous studies that related stoichiometry to the unit-cell length are also shown in Figure 7 for comparison. A robust linear trend is observed between the studies using a linear regression (R^2 = 0.92, n = 42). The fitted line yields the equation: $a = 0.1094(\pm0.0050)x_d + 8.3424(\pm0.0018)$, where $a(x_d = 0)$ = 8.3424 Å and $a(x_d = 0.5)$ = 8.3971 Å, both in excellent agreement with the reference values above. This method also validates the usage of pXRD to characterize stoichiometries of nanoparticulate magnetite between the two extremes (i.e., 0 and 0.5); although pXRD does not appear to be as precise as Mössbauer spectroscopy and acidic dissolution methods. pXRD may be a useful means for characterizing samples retroactively, and as a crude estimate when additional characterization is not possible.

The relative intensity of the (111) peak has also been used to determine stoichiometry in the past. It has been proposed that as the magnetite becomes more oxidized (lower x), the (111) peak will decrease due to octahedral vacancies (i.e., less atoms to diffract). Linear relationships have been observed in the past (Gallagher et al. 1968; Tronc et al. 1982; Volenik et al. 1975), yet some studies have noticed no correlation (Annersten and Hafner 1973; Goss 1988). As mentioned earlier, this apparent contradiction has been rationalized by the possibility that different nonstoichiometric magnetite and maghemite structures can exist, with vacancy location and structural ordering varying between samples synthesis methods (Annersten and Hafner 1973). The peak intensities were measured for the seven most intense peaks in this study, with the data summarized in Table 3. In this work, there appears to be a slight positive trend between the (111) peak intensity and magnetite stoichiometry (R^2 = 0.57, n = 7); however, the noise of the data appears to be too great. For the five x_d = 0.50 replicates, the standard deviation of (111) peak intensities was 3.1%, which was roughly the extent of change observed between the samples.

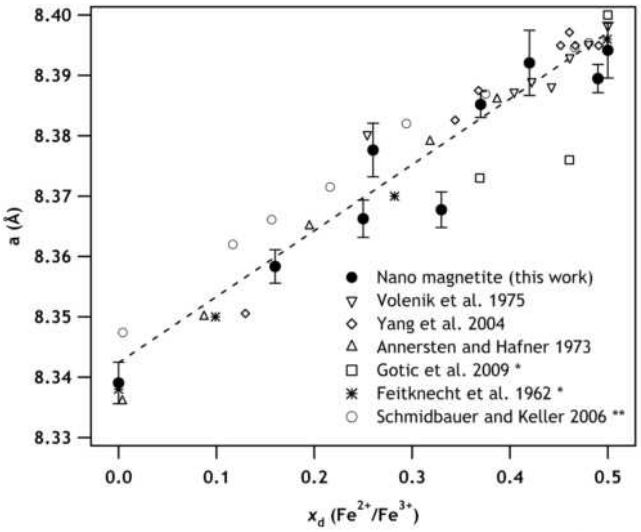

FIGURE 7. Unit-cell length of magnetite derived from fitting pXRD patterns at varying stoichiometries (x_d). Error bars shown are the standard deviations provided from the full pattern fit. For the x_d = 0.50 sample, the error bars shown are calculated from the standard deviation of five replicate samples. The fit shown is for data from all studies; $a = 0.1094(\pm0.0050)x_d + 8.3424(\pm0.0018)$; R^2 = 0.920; n = 43. A fit of the data collected in this study (line not shown) yielded a linear relationship of $a = 0.108x_d + 8.341$; R^2 = 0.914; n = 9. For literature values, x was determined by acidic dissolution except for denoted samples: for one star (*), the stoichiometry was determined using Mössbauer spectroscopy, and for two stars (**), the stoichiometry was determined by the change in mass upon oxidation.

Applicability of Mössbauer spectroscopy and pXRD for determination of stoichiometry

Here, the three most common techniques for determining magnetite stoichiometry have been validated for nanoparticulate magnetite samples on the basis that there is good agreement among the three methods. Acidic dissolution is a simple, easy method for determining stoichiometry of synthesized samples, but care must be taken to avoid oxidation by air-exposure and filtration. There are many cases, however, when acidic dissolution of the sample is not a possibility. For example, natural and mixed-phased samples can contain other redox active components (e.g., bacteria), or have functional groups adhered to the particle surface for stabilization. In these cases, spectroscopic techniques are preferred because the sample does not require any additional treatment (e.g., washing) to characterize.

One important limitation of these methods is the effect of substituent elements within the magnetite crystal lattice. For example, aluminum can be readily substituted for ^{Tet}Fe atoms, and work has shown that it will influence the relative ratios of sextets in Mössbauer spectra, the unit-cell length in pXRD, and the acidic dissolution values (Cornell and Schwertmann 2003; da Costa et al. 1996). As a result, the stoichiometry could easily be misinterpreted using these techniques, especially when applied to natural samples where the source elements are unknown. Additional characterization will thus be needed to determine the content of substituent. Furthermore, although the effects of foreign cation substitution have been explored in physical and mineralogical literature (da Costa et al. 1996; Gillot et al. 1975; Moskowitz et al. 1998; Vandenberghe and de Grave 1989), they remain largely unexplored with respect to environmentally relevant reactions (Jentzsch et al. 2007), especially with the magnetite stoichiometry in mind.

Despite this limitation, the strong trends observed among the three techniques suggest that acid dissolution, Mössbauer spectroscopy, and pXRD are all valid approaches for determining the stoichiometry of nanoparticulate samples. Discrepancies between techniques observed in previous works for larger particulate magnetite are likely in part due to the several structural forms with which nonstoichiometric magnetite and maghemite can

TABLE 2. Observed pXRD peak locations from magnetite batches with varying stoichiometries

				Nanoparticulate magnetite (x_d)								
(*hkl*)	Ref. 2θ*	Ref. d (Å)*	LP† (0.50)	0.00	0.16	0.25	0.26	0.33	0.36	0.42	0.49	0.50‡
(111)	21.29	4.8426	21.12	B.D.§	21.23	21.25	21.24	21.50	B.D.§	21.50	21.25	21.25 (0.067)‖
(220)	35.11	2.9655	34.95	35.17	35.08	35.20	35.02	35.27	34.94	35.20	35.12	34.98 (0.111)
(311)	41.43	2.5289	41.19	41.52	41.38	41.38	41.28	41.56	41.14	41.42	41.38	41.24 (0.092)
(400)	50.50	2.0969	50.27	50.66	50.41	50.31	50.38	50.68	50.22	50.58	50.44	50.33 (0.093)
(422)	62.99	1.7121	62.77	63.31	62.83	63.17	62.79	63.14	63.03	63.06	62.81	62.82 (0.129)
(511)	67.30	1.6142	67.19	67.61	67.49	67.36	67.24	67.54	67.14	67.36	67.24	67.12 (0.092)
(440)	74.21	1.4827	74.01	74.58	74.21	74.20	74.16	74.40	73.96	74.24	74.16	74.02 (0.080)
a fit# (Å)		8.3958	8.3876	8.3390	8.3584	8.3662	8.3776	8.3677	8.3852	8.3921	8.3895	8.3942
σ_a** (Å)			0.0023	0.0034	0.0028	0.0031	0.0044	0.0029	0.0022	0.0054	0.0023	(0.0046)‖

Notes: Whole pattern fits of the patterns were used to determine the magnetite unit-cell parameter (*a*).
* Nakagiri et al. (1986).
† LP = Large particulate magnetite (x_d, x_{MS} = 0.50).
‡ Values reported are the average of five identically prepared samples. Parenthetic values are the standard deviation between samples.
§ Below detection limit (<3% of maximum intensity peak).
‖ Parenthetic values are the standard deviation of five replicate samples for x = 0.50 magnetite.
Fit done using Jade 6 software (described in the Materials and Methods).
** Standard deviation of *a* from the whole pattern fit.

TABLE 3. Relative peak intensities of fitted pXRD peaks for magnetites with varying stoichiometries

			Nanoparticulate magnetite (x_d)								
(*hkl*)	Ref.*	LP†	0.00	0.16	0.25	0.26	0.33	0.36	0.42	0.49	0.50§
(111)	8.2	4.4	B.D.‡	5.0	4.7	5.7	7.4	B.D.‡	5.2	7.6	10.1 (3.1)
(220)	28.4	23.7	32.5	34.3	24.2	27.9	31.2	22.9	29.9	26.0	25.7 (2.2)
(311)	100.0	100.0	100.0	100.0	100.0	100.0	100.0	100.0	100.0	100.0	100.0 (0.0)
(400)	8.1	23.2	26.6	32.1	27.0	30.9	34.2	29.7	32.4	35.5	30.4 (2.3)
(422)	9.2	7.5	10.0	7.5	8.0	7.6	7.3	10.0	6.5	5.9	7.7 (1.2)
(511)	24.3	31.7	24.8	24.4	25.3	29.9	27.3	40.9	28.4	27.9	29.2 (7.7)
(440)	41.7	30.9	43.9	60.2	45.9	47.8	46.1	69.5	43.6	54.1	49.0 (11.0)

* Nakagiri et al. (1986).
† LP = Large particulate magnetite (x_d, x_{MS} = 0.50).
‡ Below detection limit (<3% of maximum intensity peak).
§ Values reported are the average of five identically prepared samples. Parenthetic values are the standard deviation between samples.

take. As a result, caution should be taken in further interpretation of spectra and pXRD patterns, as the Mössbauer hyperfine parameters and the (111) pXRD relative peak intensities are likely to be dependent upon factors besides stoichiometry. Acidic dissolution is thus a favorable characterization choice, as it will be independent of particle size and synthesis method, although it will not address sample impurities. The robust trend observed for the pXRD data, however, suggests that the unit-cell length (*a*) is likely directly related to stoichiometry and is thus probably immune to the influence of synthesis methods.

ACKNOWLEDGMENTS

This work was supported by a National Science Foundation NIRT grant (EAR-0506679). The manuscript was greatly improved by the comments of three anonymous reviewers.

REFERENCES CITED

Annersten, H. and Hafner, S.S. (1973) Vacancy distribution in synthetic spinels of the series magnetite-γ-iron(III) oxide. Zeitschrift für Kristallographie, 137, 321–340.

Antonov, V.N., Harmon, B.N., and Yaresko, A.N. (2003) Electronic structure and X-ray magnetic circular dichroism in Fe_3O_4 and Mn-, Co-, or Ni-substituted Fe_3O_4. Physical Review B, 67, 024417.

Carvallo, C., Sainctavit, P., Arrio, M.-A., Menguy, N., Wang, Y., Ona-Nguema, G., and Brice-Profeta, S. (2008) Biogenic vs. abiogenic magnetite nanoparticles: A XMCD study. American Mineralogist, 93, 880–885.

Cornell, R.M. and Schwertmann, U. (2003) The Iron Oxides: Structure, properties, reactions, occurrence, and uses. VCH, New York.

Cullen, J.R. and Callen, E. (1970) Collective electron theory of metal-semiconductor transition in magnetite. Journal of Applied Physics, 41, 879–880.

Cullen, A.C., Vorhees, D.J., and Altshul, L.M. (1996) Influence of harbor contamination on the level and composition of polychlorinated biphenyls in produce in greater New Bedford, Massachusetts. Environmental Science and Technology, 30, 1581–1588.

da Costa, G.M., De Grave, E., de Bakker, P.M.A., and Vandenberghe, R.E. (1995) Influence of nonstoichiometry and the presence of maghemite on the Mössbauer spectrum of magnetite. Clays and Clay Minerals, 43, 656–668.

da Costa, G.M., De Grave, E., and Vandenberghe, R.E. (1996) Mössbauer studies of magnetite and Al-substituted maghemites. Hyperfine Interactions, 117, 207–243.

Daniels, J.M. and Rosencwaig, A. (1969) Mössbauer spectroscopy of stoichiometric and non-stoichiometric magnetite. Journal of Physics and Chemistry of Solids, 30, 1561–1571.

Degrave, E., Persoons, R.M., Vandenberghe, R.E., and de Bakker, P.M.A. (1993) Mossbauer study of the high-temperature phase of Co-substituted magnetites, $Co_xFe_{3-x}O_4$. I. x≤0.04. Physical Review B, 47, 5881–5893.

Feitknecht, W., Brunner, P., and Oswald, H.R. (1962) Uber Den Einfluss Der Feuchtigkeit Auf Die Oxydation Von Manganhydroxid Durch Molekularen Sauerstoff. Zeitschrift für Anorganische und Allgemeine Chemie, 316, 154–160.

Ferrey, M., Wilkin, R., Ford, R., and Wilson, J. (2004) Nonbiological removal of cis-dichloroethylene and 1,1-dichlorethylene in aquifer sediment containing magnetite. Environmental Science and Technology, 38, 1746–1752.

Gallagher, K.J., Feitknecht, W., and Mannweiler, U. (1968) Mechanism of oxidation of magnetite to γ-Fe_2O_3. Nature, 217, 1118–1121.

Garcia, J. and Subias, G. (2004) The Verwey transition—A new perspective. Journal of Physics: Condensed Matter, 16, R145–R178.

Gillot, B., Tyranowicz, J., and Rousset, A. (1975) Study of kinetics of oxidation of finely divided magnetite. 1. Influence of aluminum substitution. Materials Research Bulletin, 10, 775–782.

Gorski, C.A. and Scherer, M.M. (2009) Influence of magnetite stoichiometry on Fe^{II} uptake and nitrobenzene reduction. Environmental Science and Technology, 43, 3675–3680.

Gorski, C.A., Nurmi, J.T., Tratnyek, P.G., Hofstetter, T.B., and Scherer, M.M. (2010) Redox behavior of magnetite: Implications for contaminant reduction. Environmental Science and Technology, 44, 55–60.

Goss, C.J. (1988) Saturation magnetization, coercivity, and lattice parameter changes in the system Fe_3O_4-γFe_2O_3, and their relationship to structure. Physics and Chemistry of Minerals, 16, 164–171.

Gotic, M., Koscec, G., and Music, S. (2009) Study of the reduction and reoxidation of substoichiometric magnetite. Journal of Molecular Structure, 924–26, 347–354.

Haggstrom, L., Annersten, H., Ericsson, T., Wappling, R., Karner, W., and Bjarman, S. (1978) Magnetic dipolar and electric quadrupolar effects on the Mössbauer spectra of magnetite above the Verwey transition. Hyperfine Interactions, 5,

201–214.
Hansel, C.M., Benner, S.G., and Fendorf, S. (2005) Competing Fe(II)-induced mineralization pathways of ferrihydrite. Environmental Science and Technology, 39, 7147–7153.
Hansen, H.C.B. (1989) Composition, stabilization, and light-absorption of Fe(II) Fe(III) hydroxy-carbonate (green rust). Clay Minerals, 24, 663–669.
Howard, S.A. and Preston, K.D. (1989) Profile fitting of powder diffraction patterns. In D.L. Bish and J.E. Post, Eds., Modern Powder Diffraction, 20, p. 217–275. Reviews in Mineralogy, Mineralogical Society of America, Chantilly, Virginia.
Ihle, D. and Lorenz, B. (1985) Small-polaron band vs. hopping conduction in Fe_3O_4. Journal of Physics C: Solid State Physics, 18, L647–L650.
Itai, R., Shibuya, M., Matsumura, T., and Ishi, G. (1971) Electrical resistivity of magnetite anodes. Journal of the Electrochemical Society, 118, 1709–1711.
Jentzsch, T.L., Chun, C.L., Gabor, R.S., and Penn, R.L. (2007) Influence of aluminum substitution on the reactivity of magnetite nanoparticles. Journal of Physical Chemistry C, 111, 10247–10253.
Jolivet, J.P. and Tronc, E. (1988) Interfacial electron transfer in colloidal spinel iron oxide. Conversion of Fe_3O_4-γFe_2O_3 in aqueous solution. Journal of Colloid and Interface Chemistry, 125, 688–701.
Jolivet, J.P., Belleville, P., Tronc, E., and Livage, J. (1992) Influence of Fe(II) on the formation of the spinel iron oxide in alkaline medium. Clays and Clay Minerals, 40, 531–539.
Kuhn, L.T., Bojesen, A., Timmermann, L., Nielsen, M.M., and Morup, S. (2002) Structural and magnetic properties of core-shell iron-iron oxide nanoparticles. Journal of Physics: Condensed Matter, 14, 13551–13567.
Lagarec, K. and Rancourt, D.G. (1997) Extended Voigt-based analytic lineshape method for determining N-dimensional correlated hyperfine parameter distributions in Mössbauer spectroscopy. Nuclear Instruments and Methods in Physical Research B, 129, 266–280.
Lee, W. and Batchelor, B. (2002) Abiotic reductive dechlorination of chlorinated ethylenes by iron-bearing soil minerals. 1. Pyrite and magnetite. Environmental Science and Technology, 36, 5147–5154.
Lotgering, F.K. and Vandiepen, A.M. (1977) Electron exchange between Fe^{2+} and Fe^{3+} ions on octahedral sites in spinels studied by means of paramagnetic Mössbauer spectra and susceptibility measurements. Journal of Physics and Chemistry of Solids, 38, 565–572.
McCormick, M.L., Bouwer, E.J., and Adriaens, P. (2002) Carbon tetrachloride transformation in a model iron-reducing culture: Relative kinetics of biotic and abiotic reactions. Environmental Science and Technology, 36, 403–410.
Morrall, P., Schedin, F., Case, G.S., Thomas, M.F., Dudzik, E., van der Laan, G., and Thornton, G. (2003) Stoichiometry of $Fe_{3-\delta}O_4$(111) ultrathin films on Pt(111). Physical Review B, 67, 214408.
Morrish, A.H., Haneda, K., and Schurer, P.J. (1976) Surface magnetite structure of small γ-Fe_2O_3 particles. Journal de Physique, 12, 301–305.
Moskowitz, B.M., Jackson, M., and Kissel, C. (1998) Low-temperature magnetic behavior of titanomagnetites. Earth and Planetary Science Letters, 157, 141–149.
Nakagiri, N., Manghnani, M.H., Ming, L.C., and Kimura, S. (1986) Crystal structure of magnetite under pressure. Physics and Chemistry of Minerals, 13, 238–244.
Ozdemir, O., Dunlop, D.J., and Moskowitz, B.M. (1993) The effect of oxidation on the Verwey transition in magnetite. Geophysical Research Letters, 20, 1671–1674.
Pankhurst, Q.A., Connolly, J., Jones, S.K., and Dobson, J. (2003) Applications of magnetic nanoparticles in biomedicine. Journal of Physics D: Applied Physics, 36, R167–R181.
Peterson, M.L., White, A.F., Brown, G.E., and Parks, G.A. (1997) Surface passivation of magnetite by reaction with aqueous Cr(VI): XAFS and TEM results. Environmental Science and Technology, 31, 1573–1576.
Ping, J.Y. and Rancourt, D.G. (1994a) An effective method of direct QSD extraction using combined partial deconvolution. Hyperfine Interactions, 92, 1203–1207.
——— (1994b) Failure of the direct HFD extraction method. Hyperfine Interactions, 92, 1209–1212.
Raj, K. and Moskowitz, R. (1990) Commercial applications of ferrofluids. Journal of Magnetism and Magnetic Materials, 85, 233–245.
Ramdani, A., Steinmetz, J., Gleitzer, C., Coey, J.M.D., and Friedt, J.M. (1987) Perturbation de l'echange electronique rapide par les lacunes cationiques dans $Fe_{3-x}O_4$ ($x < 0{,}09$). Journal of Physics and Chemistry of Solids, 48, 217–228.
Rancourt, D.G. and Ping, J.Y. (1991) Voigt-based methods for arbitrary-shape static hyperfine parameter distributions in Mössbauer spectroscopy. Nuclear Instruments and Methods in Physics Research B, 58, 85–97.
Reynolds, R.J. (1989) Diffraction by small and disordered crystals. In D.L. Bish and J.E. Post, Eds., Modern Powder Diffraction, 20, p. 145–182. Reviews in Mineralogy, Mineralogical Society of America, Chantilly, Virginia.
Sawatzky, G.A., Coey, J.M.D., and Morrish, A.H. (1969) Mössbauer study of electron hopping in octahedral sites of Fe_3O_4. Journal of Applied Physics, 40, 1402–1403.
Schmidbauer, E. and Keller, M. (2006) Magnetic hysteresis properties, Mössbauer spectra and structural data of spherical 250 nm particles of solid solutions Fe_3O_4-γ-Fe_2O_3. Journal of Magnetism and Magnetic Materials, 297, 107–117.
Schwertmann, U. and Cornell, R.M. (1991) Iron Oxides in the Laboratory, 137 p. VCH, Weinheim.
Scott, T.B., Allen, G.C., Heard, P.J., and Randell, M.G. (2005) Reduction of U(VI) to U(IV) on the surface of magnetite. Geochimica et Cosmochimica Acta, 69, 5639–5646.
Sherman, D.M. (1987) Molecular orbital (SCF-Xα-SW) theory of metal-metal charge transfer processes in minerals. Physics and Chemistry of Minerals, 14, 355–363.
Stockbridge, C.D., Sewell, P.B., and Cohen, M. (1961) Cathodic behavior of iron single crystals and the oxides Fe_3O_4, γ-Fe_2O_3, and α-Fe_2O_3. Journal of the Electrochemical Society, 108, 928–933.
Stratmann, M., Bohnenkamp, K., and Engell, H.-J. (1983) An electrochemical study of phase-transitions in rust layers. Corrosion Science, 23, 969–985.
Tamaura, Y., Ito, K., and Katsura, T. (1983) Transformation of γ-FeO(OH) to Fe_3O_4 by adsorption of iron(II) ion on γ-FeO(OH). Journal of the Chemical Society, Dalton Transactions, 2, 189–194.
Tamura, H., Goto, K., Yotsuyan, T., and Nagayama, M. (1974) Spectrophotometric determination of iron(II) with 1,10-phenanthroline in presence of large amounts of iron(III). Talanta, 21, 314–318.
Tronc, E., Jolivet, J.P., and Massart, R. (1982) Defect spinel structure in iron oxide colloids. Materials Research Bulletin, 17, 1365–1369.
Tronc, E., Jolivet, J.P., Belleville, P., and Livage, J. (1989) Redox phenomena in spinel iron-oxide colloids induced by adsorption. Hyperfine Interactions, 46, 637–643.
Tronc, E., Belleville, P., Jolivet, J.P., and Livage, J. (1992) Transformation of ferric hydroxide into spinel by Fe(II) adsorption. Langmuir, 8, 313–319.
Vandenberghe, R.E. and de Grave, E. (1989) Mössbauer effect studies of oxidic spinels. In G.J. Long, Ed., Mössbauer Spectroscopy Applied to Inorganic Chemistry, 3, p. 59–182. Plenum Press, New York.
Vandenberghe, R.E., Hus, J.J., and de Grave, E. (1998) Evidence from Mössbauer spectroscopy of neo-formation of magnetite/maghemite in the soils of loess/paleosol sequences in China. Hyperfine Interactions, 117, 359–369.
Vandenberghe, R.E., Barrero, C.A., da Costa, G.M., Van San, E., and de Grave, E. (2000) Mössbauer characterization of iron oxides and (oxy)hydroxides: The present state of the art. Hyperfine Interactions, 126, 247–259.
Verwey, E.J.W. and Haayman, P.W. (1941) Electronic conductivity and transition point of magnetite (Fe_3O_4). Physica, 8, 979–987.
Vikesland, P.J., Heathcock, A.M., Rebodos, R.L., and Makus, K.E. (2007) Particle size and aggregation effects on magnetite reactivity toward carbon tetrachloride. Environmental Science and Technology, 41, 5277–5283.
Volenik, K., Seberini, M., and Neid, J. (1975) Mössbauer and X-ray-diffraction study of nonstoichiometry in magnetite. Czechoslovak Journal of Physics, 25, 1063–1071.
Walz, F. (2002) The Verwey transition—A topical review. Journal of Physics: Condensed Matter, 14, R285–R340.
White, A.F. and Peterson, M.L. (1996) Reduction of aqueous transition metal species on the surfaces of Fe(II)-containing oxides. Geochimica et Cosmochimica Acta, 60, 3799–3814.
White, A.F., Peterson, M.L., and Hochella, M.F. (1994) Electrochemistry and dissolution kinetics of magnetite and ilmenite. Geochimica et Cosmochimica Acta, 58, 1859–1875.
Yang, J.B., Zhou, X.D., Yelon, W.B., James, W.J., Cai, Q., Gopalakrishnan, K.V., Malik, S.K., Sun, X.C., and Nikles, D.E. (2004) Magnetic and structural studies of the Verwey transition in $Fe_{3-\delta}O_4$ nanoparticles. Journal of Applied Physics, 95, 7540–7542.
Yavuz, C.T., Mayo, J.T., Yu, W.W., Prakash, A., Falkner, J.C., Yean, S., Cong, L.L., Shipley, H.J., Kan, A., Tomson, M., Natelson, D., and Colvin, V.L. (2006) Low-field magnetic separation of monodisperse Fe_3O_4 nanocrystals. Science, 314, 964–967.

MANUSCRIPT RECEIVED OCTOBER 26, 2009
MANUSCRIPT ACCEPTED FEBRUARY 9, 2010
MANUSCRIPT HANDLED BY JOSHUA FEINBERG